# Energy Definition and Minimization in Avalanche Models for Solar Flares

**Henri Lamarre**[1]•• · **Paul Charbonneau**[1]•• ·
**Antoine Strugarek**[2]••

© **Springer** ••••

## Abstract

Self-organised critical avalanche models are a class of cellular automata that, despite their simplicity, can be applied to the modeling of solar (and stellar) flares and generate robust power-law distributions in event size measures. However, bridging the conceptual gap to both magnetohydrodynamics and real flare observations continues to prove challenging. In this paper, we focus on a specific, key aspect of this endeavour, namely the definition of magnetic energy and its consequences for the model's internal dynamics and energy release statistics. We show that the dual requirement of releasing energy and restoring local stability demands that the instability criterion and boundary conditions be set in a manner internally consistent with a given energy definition, otherwise unphysical behavior ensues, e.g., negative energy release. Working with three energy definitions previously used in the literature, we construct such internally consistent avalanche models and compare/contrast their energy release statistics. Using the same set of models, we also explore a recent proposal by Farhang et al. (2018, 2019), namely that avalanches/flares should maximize the amount of energy released by the lattice when instabilities are triggered. This tends to produce avalanches of shorter duration but higher peak energy release, but adding up to similar total energy release. For the three energy definition we tested, such avalanche models exhibit almost identical distributions of event size measures. Our results indicate that the key to reproduce solar-like power-law slopes in these

✉ HLamarre
henri.lamarre@umontreal.ca

P. Charbonneau
paul.charbonneau@umontreal.ca

A. Strugarek
antoine.strugarek@cea.fr

[1]    Physics Department, Université de Montréal, CP 6128 Centre-Ville, Montréal, Qc H3C-3J7, Canada

[2]    Université Paris-Saclay, Université Paris Cité, CEA, CNRS, AIM, 91191, Gif-sur-Yvette, France

size measures is lattice configurations in which most nodes remain relatively far from the instability threshold.

**Keywords:** Avalanche models - Solar Flares

## 1. Introduction

Many natural physical systems exhibit energy loading and release spanning a very wide range of characteristic spatiotemporal scales. Examples include landslides, forest fires, earthquakes, geomagnetic substorms, as well as solar and stellar flares (see, e.g. Aschwanden, 2011, Chapter 1). In such physical systems, the buildup of energy is a slow, continuous process, while its release is rapid and spatiotemporally intermittent, with size measures of energy release events distributed over many orders of magnitude.

Even if the underlying governing physical laws are known, the computational modelling of such multiscale systems is extremely arduous in practice. Direct numerical simulations typically compromise on the range of scales modelled, by truncation at either or both the low and high ends of the scale. These truncated scales can then be modeled via subgrid models or boundary conditions, respectively (Shibata and Magara, 2011). When this approach is not feasible, one must turn to simplifications at the level of the system geometry and/or governing physics. Lattice-based models represent an extreme example of this latter approach.

Simply put, a lattice model is a network of interconnected nodes, each characterized by a state (or value) which evolves discretely in time according to an update rule determined by the state of other nodes to which it is connected. The so-called avalanche (or sandpile) models are a class of lattice-based models which has proven robust generators of discrete energy release events patterns exhibiting scale-invariant power-law statistics in their size measures. A particularly interesting class of such avalanche models are those exhibiting Self-Organised Criticality (hereafter SOC: see, e.g. Bak, Tang, and Wiesenfeld, 1988; Jensen, 1998; Aschwanden, 2013). This refers to systems in which the statistical equilibrium state generating scale-invariant behavior is an attractor of the internal dynamics, and thus is reached and sustained without the need to fine tune the external driver or internal model parameters.

The application of such SOC avalanche models to solar flares was initiated by the seminal work of Lu and Hamilton (1991), and was successful in robustly reproducing the observed power-law form of the statistical distribution of event size measures (Dennis, 1985, see also Lu *et al.* 1993). This success continues to motivate the search for a convincing physical underpinning of the loading, instability and redistribution rules for the nodal variable defined over the lattice (Lu, 1995a; Isliker *et al.*, 1998; Isliker, Anastasiadis, and Vlahos, 2000; Liu *et al.*, 2002; Farhang, Safari, and Wheatland, 2018, see also Aschwanden 2013, Chapter 12).

The majority of extant SOC avalanche models for solar and stellar flares have adopted a Lu & Hamilton-like modelling framework. A nodal variable related

to the magnetic field is defined on a Cartesian grid with nearest-neighbour connectivity, and evolves according to loading, stability and local redistribution rules through synchronous lattice updating (but do see, e.g., Hughes *et al.*, 2003; Morales and Charbonneau, 2008; López Fuentes and Klimchuk, 2010, for examples of SOC flare models using fieldlines as dynamical elements).

However designed, all such models leave a good measure of arbitrariness in computing quantitative model output of the type that can be compared to observations. Some *sine qua non* constraints are nonetheless generally agreed upon. Observations have established unambiguously that flaring taps into magnetic energy of coronal magnetic structures overlaying active regions; any redistribution rule should thus reduce the energy content of the lattice. Flare onset is generally believed to result from magnetic reconnection, itself triggered by magnetohydrodynamic (MHD) and/or plasma instabilities. In the Parker nanoflare scenario, the participating instability is associated with a threshold in the electrical current density at sites of magnetic tangential discontinuities. Under this *Ansatz* the redistribution rules should decrease the local current density at the unstable lattice nodes.

These matters become of the utmost importance when using avalanche models to carry out flare prediction (Bélanger, Vincent, and Charbonneau, 2007; Strugarek and Charbonneau, 2014; Thibeault *et al.*, 2022). A physically well-motivated measure of energy is essential to define appropriate redistribution rules, and, in a data assimilation and prediction context, to match the model's energy release time series to observations, as done for example by Thibeault *et al.* (2022) with GOES X-Ray flux time series. The definition of lattice energy, in turn, is critically dependent on the physical identification of the dynamical variable defined at lattice nodes and redistributed in the course of avalanches.

We begin in Section 2 by reviewing the design of the Lu *et al.* (1993) avalanche model, and a plausible physical interpretation that can be placed on its components and dynamical rules. We introduce in Section 3 two "better" definitions of lattice energy, and in Section 4 we demonstrate how to design sandpile instability rules coherent with these new energy definitions, and investigate the resulting energy release statistics. In Section 5, using these consistent energy/stability definitions, we explore the behavior of the Lu *et al.* (1993) model under the hypothesis that redistribution during avalanches must maximize energy release, as proposed originally by Farhang, Safari, and Wheatland (2018). We close in Section 6 by summarizing our findings in the context of the design of internally consistent lattice models of solar flares.

## 2. The Lu & Hamilton model

### 2.1. A Reference Model

The avalanche model used throughout this paper is that originally designed by Lu and Hamilton (1991), more specifically the version described in Lu *et al.* (1993) (hereafter L93; see also Charbonneau *et al.* 2001). The model is built on a Cartesian lattice with von Neumann nearest-neighbour connectivity, with the

nodal variable identified with the magnetic vector potential $\mathbf{A}$. For reasons to be described presently, we depart from L93 in considering a two-dimensional lattice and a single scalar component $A_{i,j}$ of the vector potential as nodal variable, the latter producing a similar avalanching behavior as the vector nodal variable originally introduced by L93 in view of the adopted driving scheme (Robinson, 1994).

Following L93, the lattice is driven by sequentially adding small increments $\delta A$ at randomly selected lattice nodes, with $\delta A$ extracted from a uniform distribution of random deviates spanning the range $[-0.2, 0.8]$, and $A_{i,j} = 0$ enforced at boundary nodes at all times. As the driving gradually builds up the nodal variable on the lattice, its curvature is monitored by computing, at each node:

$$\Delta A_{i,j} = A_{i,j} - \frac{1}{4} \sum_{N_1} A_{N_1}, \tag{1}$$

with the index $N_1$ running over the four nearest neighbors:

$$N_1 \equiv [(i+1,j), (i-1,j), (i,j-1), (i,j+1)]. \tag{2}$$

A node is deemed unstable when $\Delta A_{i,j}$ exceeds a preset threshold $Z_c$:

$$|\Delta A_{i,j}| > Z_c. \tag{3}$$

When this condition is satisfied at any one node, driving stops and a portion of the nodal variable at node $(i,j)$ is transferred isotropically to its nearest neighbors according to the redistribution rule:

$$A'_{i,j} = A_{i,j} - \frac{4}{5}Z, \qquad A'_{N_1} = A_{N_1} + \frac{1}{5}Z, \qquad Z = \text{sign}(\Delta A_{i,j})Z_c, \tag{4}$$

where primes indicate post-redistribution values. This redistribution rule conserves the nodal variable, and it is easily shown that it reduces the curvature measure (1) by an amount $Z_c$, which restores stability at node $(i,j)$ provided $\Delta A_{i,j} < 2Z_c$, which imposes the constraint $\delta A/Z_c < 1$ on the size of the driving increment.

While stability is thus restored at the formerly unstable node, the redistribution process may force one or more of the nearest neighbour nodes to exceed the instability threshold (3), in which case the redistribution rules (4) are applied again to newly unstable node(s), and so on, in avalanching manner, until stability is restored across the whole lattice, at which point driving resumes.

Under these evolutionary rules the system eventually reaches a statistically stationary self-organised critical state, characterized by scale-free avalanches of size ranging from a single node to the whole lattice, unfolding in the outer layer of a "sandpile" of nodal variable of approximately parabolic shape in both lattice direction and peaking at lattice center (see, e.g., Section 2 in Charbonneau *et al.*, 2001).

## 2.2. Physical Interpretation

Building on LH93 (see also Lu 1995b), and inspired also by the coronal heating scenario by nanoflares developed by Parker (1988), Strugarek *et al.* (2014) propose a specific interpretative physical picture, which is also adopted in what follows. The 2D lattice is viewed as a perpendicular section of a coronal loop taken at its apex, where flare onset is often observed (see, e.g., Tsuneta *et al.*, 1992; Masuda *et al.*, 1994), with the magnetic field then dominated by its axial component ($B_z$, say). With the nodal variable identified with the $z$-component of the vector potential, its curl then defines the deviation of the magnetic field from the axial direction, i.e., the twisting and braiding of magnetic-field lines about each other. If the twist angle is small —Parker (1988) estimates it at $\simeq 14°$,— then both $\mathbf{A}$ and $\mathbf{B}$ are dominated by their $z$-component, in which case the electrical current density $\mathbf{J}$ can be approximated as

$$\mu_0 \mathbf{J} = \nabla \times \mathbf{B} \simeq \nabla \times \nabla \times (A_z \hat{\mathbf{z}}) = -\nabla_\perp^2 A_z, \tag{5}$$

under the Coulomb gauge $\nabla \cdot \mathbf{A} = 0$, and with the Laplacian $\nabla_\perp^2$ defined in the cross-sectional plane, i.e., perpendicular to the loop axis.

Under this interpretation, the addition of an increment $\delta A$ at a node amounts to an increase of the local twist (Lu *et al.*, 1993), and the stability measure $\Delta A_{i,j}$ defined via Equation 1 can be interpreted as a second-order centered finite difference representation of the 2D Laplacian. If that interpretation is accepted[1], then the instability condition (3) becomes a threshold on the magnitude of the electrical current density, which is physically satisfying if the energy released by avalanches is taken through occur via magnetic reconnection triggered by plasma instabilities.

## 2.3. Defining Magnetic Energy

A proper definition of the magnetic-energy content ($E$) of the lattice is clearly crucial in trying to bridge the gulf between such simple avalanches models and actual solar (or stellar) flares. If the nodal variable is identified with the magnetic field itself, as done originally in Lu and Hamilton (1991), then unambiguously $E \propto \sum \mathbf{B}^2$ over all lattice nodes. However, under such an identification, the solenoidal constraint $\nabla \cdot \mathbf{B} = 0$ is not necessarily satisfied by the set of forcing and redistribution rules described in Section 2.1. Identifying instead the nodal variable with the magnetic-vector potential satisfies the solenoidal constraint by construction, but the definition of lattice energy becomes trickier.

---

[1]This has been common practice in attempts to bridge the gap between MHD and lattice models of flares (e.g. Isliker, Anastasiadis, and Vlahos, 2000; Liu *et al.*, 2002; Strugarek *et al.*, 2014). However, lattice models are fundamentally discrete systems, and in general the state of a node should not be interpreted as a continuous variable sampled on a computational mesh; in particular, because the nodal quantity varies discretely from one node to the next, finite difference expressions of derivatives diverge, rather than converge, as the grid spacing tends to zero. We nonetheless proceed with the interpretation of lattice model rules in terms of centered finite difference on the lattice.

In our adopted physical picture, the magnetic field components in the plane of the lattice is $\mathbf{B}_\perp \propto \nabla \times (A_z \mathbf{e_z})$. With $B_z$ fixed by conservation of magnetic flux in the loop's cross-section, the contribution of $B_x, B_y$ to the magnetic energy is $(\nabla \times (A_z \mathbf{e_z}))^2$. If the redistribution/reconnection simply reduces the local twist without altering the global magnetic configuration, then one would expect $\sum A_{i,j}^2$ to be a good proxy for the lattice magnetic energy available for flaring[2]. This is the magnetic energy definition adopted in LH93 and many subsequent works (e.g. Lu *et al.*, 1993; Georgoulis and Vlahos, 1998; Strugarek and Charbonneau, 2014; Morales and Santos, 2020; Thibeault *et al.*, 2022):

$$E_A = \sum_{i,j} A_{i,j}^2. \tag{6}$$

Here and in the forthcoming alternate expressions for lattice energy, we have omitted the usual $1/2\mu_0$ prefactor, which amounts to rescaling energy units.

Under this definition of magnetic energy, it is a simple matter to show that the redistribution rule (4) not only restores stability, but also reduces the lattice energy, as it should in the flaring context. Specifically, with lattice energy $\propto \sum A^2$, the energy content of the five nodes involved in the redistribution rule (4) drops by

$$\Delta E_A = \frac{4}{5} Z_c \left( 2|\Delta A_{i,j}| - Z_c \right), \tag{7}$$

as detailed in appendix A.2. Setting $\Delta A_{i,j} = Z_c$, i.e., a node just reaching the instability threshold, sets the smallest amount ($e_0$) of energy that can be released by the system:

$$e_0 = \frac{4}{5} Z_c^2. \tag{8}$$

From Equation 7, the requirement that $\Delta E_A > 0$ translates into the constraint

$$|\Delta A_{i,j}| > \frac{1}{2} Z_c, \tag{9}$$

which is less constraining on $|\Delta A_{i,j}|$ than the original instability criterion of the LH93 model, as per Equation 3. Reducing curvature significantly below the stability threshold, i.e. hysteresis, is actually required for energy to slowly accumulate in the lattice, and to be subsequently released by scale-free avalanches (Lu, 1995b).

---

[2]In our geometrical interpretation of the 2D lattice (Section 2.2), the flux perpendicular to the lattice plane must be conserved. Therefore, if the redistribution alters only the degree of local twist, set by $B_x$ and $B_y$, and not the local $B_z$, then the contribution of $B_z$ to lattice energy never changes, and the "free energy" of the magnetic field is associated entirely with its components in the plane of the lattice.

## 3. Alternative Energy Definitions in the L93 Model

The most natural definition of magnetic energy is

$$E_B = \sum_{i,j} \mathbf{B}_{i,j}^2. \tag{10}$$

As argued in Section 2.3, in our geometrical setup only the magnetic energy associated with the magnetic-field components in the lattice plane can be tapped into to release energy. In this context, the magnetic vector potential is only directed along $z$ and is denoted $\mathbf{A} = A\mathbf{e}_z$. We set $A$ to be the nodal variable, and the magnetic energy contribution of the field components at node $(i, j)$ can be computed with (assuming unit grid spacing in the lattice plane):

$$
\begin{aligned}
\mathbf{B}^2 &\equiv (\nabla \times \mathbf{A})^2 \\
&= \left(-\frac{\partial A}{\partial x}\right)^2 + \left(\frac{\partial A}{\partial y}\right)^2 \\
&= \left(\frac{A_{i-1,j} - A_{i+1,j}}{2}\right)^2 + \left(\frac{A_{i,j-1} - A_{i,j+1}}{2}\right)^2.
\end{aligned}
\tag{11}
$$

In the context of our adopted geometrical picture (Section 2.2), both the magnetic field and vector potential are dominated by their $z$-component. This allows an alternate definition of magnetic energy, as recently proposed by Farhang, Safari, and Wheatland (2018). Starting from the vector identity

$$\nabla \cdot (\mathbf{A} \times \mathbf{B}) = \mathbf{B} \cdot \nabla \times \mathbf{A} - \mathbf{A} \cdot \nabla \times \mathbf{B}, \tag{12}$$

If $\mathbf{A}$ and $\mathbf{B}$ are parallel the LHS vanishes, so that

$$\mathbf{B} \cdot \mathbf{B} = \mathbf{A} \cdot (\nabla \times \mathbf{B}) = \mu_0 \mathbf{A} \cdot \mathbf{J} \simeq \mu_0 A_z J_z, \tag{13}$$

as per Ampère's Law. This provides yet another definition of energy:

$$E_{AJ} \equiv \sum_{i,j} A_{i,j} J_{i,j}, \tag{14}$$

with the $z$-component of the electrical current density computed via Equation 5 invoking again second-order centered finite differences with unit grid spacing:

$$\mu_0 J_{i,j} = 4A_{i,j} - (A_{i-1,j} + A_{i+1,j} + A_{i,j-1} + A_{i,j-1}). \tag{15}$$

Note that this third energy definition has the peculiarity that a node can potentially contribute *negatively* to magnetic energy, since $J_z$ can be of either sign, while $A_z$ is a positive quantity in our lattice model setup.

Equations 6, 10–11 and 14–15 thus offer three distinct energy definitions, which should be operationally equivalent under the assumptions underlying our geometrical/physical setup *and* provided one accepts again the use of centered finite differences on the lattice as a means of calculating the magnetic field and current density from the nodal vector potential.

Figure 1 tests this equivalence by plotting against one another avalanche energies calculated a posteriori using our three energy definitions, working off a simulation run of the LH93 model on a $64 \times 64$ lattice, already in the statistically stationary SOC state. All three correlation plots show considerable scatter for
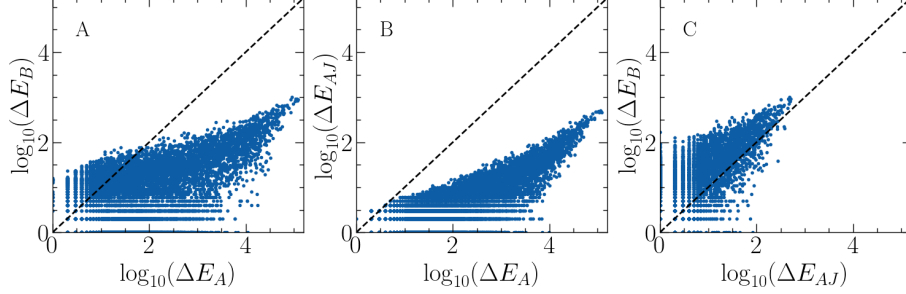


**Figure 1.** Comparison of the energy dissipated by avalanches generated by the LH93 model for each energy definition. The scales are logarithmic.

the smaller avalanches, but a good correlation emerges for the larger avalanches, which is certainly encouraging. That energy measures based on $B^2$ or $AJ$ are systematically below those based on $A^2$ was to be expected, considering that under definitions (10) and (14) it is possible for a node to contribute zero to lattice energy, or even a negative quantity in the case of energy definition (14), which is not the case with the original definition (6). Notably, the released energy on panel (C) aligns with $\Delta E_B = \Delta E_{AJ}$ (dashed diagonal) quite closely, which gives confidence in the finite difference representation of derivatives used in the two alternate energy definitions introduced in this section, since these definitions should be identical under exact mathematics and under the assumptions that $\mathbf{B}$ is dominated by its $z$-component.

Unfortunately, a serious problem emerges upon closer scrutiny. Figure 2A shows a $10^4$ iterations long segment of lattice energy time series, for the same simulation used to generate the data plotted on Figure 1. The segments are color-coded according to the energy definition used, and have each been normalized to their average value over the plotted interval to facilitate visual comparison. All three time series follow the same overall trend, but the differences betray a fundamental inconsistency in the a posteriori calculations of lattice energy using the alternate definitions (10) and (14). Figure 2B,C reproduce a $10^3$ iterations subsegment, indicated by the boxed area in panel (A), together with the time series of energy release for the three energy definitions, the latter computed as the variation in lattice energies at subsequent temporal iterations. This selected subsegment spans a large avalanche beginning at $t \simeq 6000$. All three lattice energy time series undergo a substantial drop over the course of this large avalanche, but there are many iterations within the avalanche where the lattice energy, when computed with the $B^2$ or $AJ$ definition, is *increasing* (e.g., around $t \simeq 6300$ for $E_B$ and $E_{AJ}$) rather than decreasing, as it should and as it indeed does for the $A^2$ energy definition (6). This then leads to unphysical *negative* energy release.
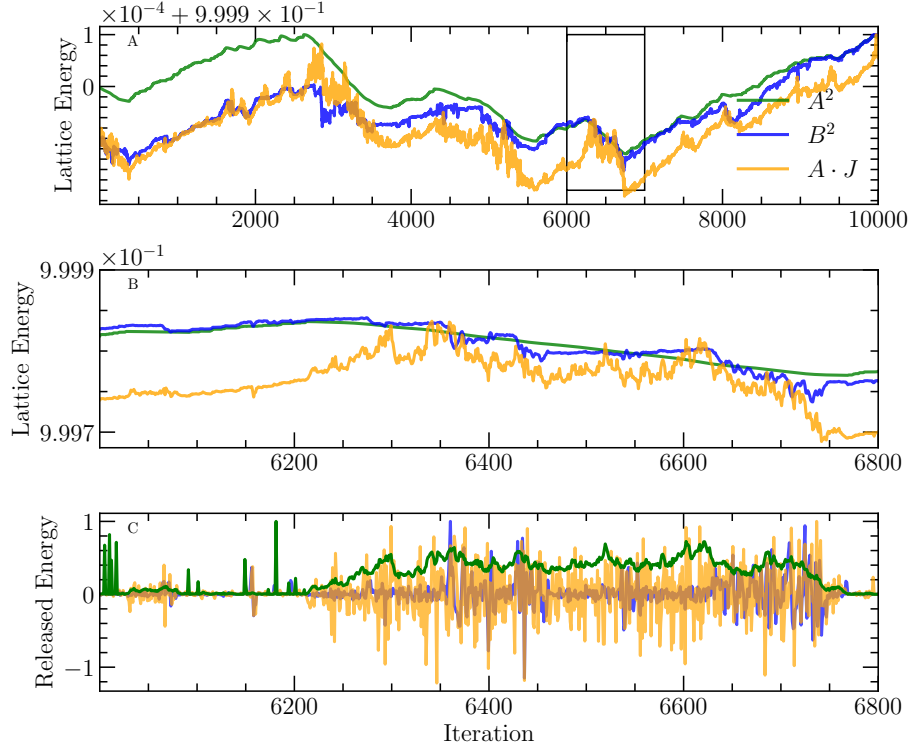
**Figure 2.** Panel (A): evolution of the normalized lattice energy for the LH model using the different energy definitions (6), (10), and (14), plotted in green, blue and orange respectively. The time series segments have each been normalized by their respective maximum values. Panel (B): 1000-iteration closeup on the boxed area on panel (A). Panel (C): Normalized energy dissipated by the models during the time series on panel (B). The dissipated energy is the lattice energy difference for avalanching iterations and is 0 otherwise.

This pathology arises from the fact that if the alternate energy definitions (10)–(11) or (14)–(15) are used in a model whose avalanching dynamics is governed by the stability criterion (1) and redistribution rule (4), it is no longer always the case that a redistribution that restores stability necessarily reduces lattice energy, or that a rule that decreases lattice energy necessarily restores stability. In other words, using an energy definition while using the stability criterion based on another energy definition creates cases where unstable nodes are unable to redistribute and/or avalanches release negative energy. Farhang, Safari, and Wheatland (2018) encountered this problem and as a consequence had to introduce additional *ad hoc* constraints on their redistribution rules. Another possibility is to change either (or both) the redistribution rules or stability criterion. We opt for the latter in what follows.

## 4. The Impact of Choosing an Energy Definition

### 4.1. Constructing the Models

In contrast to the energy definition (6), which is purely local in the nodal variable, under the two alternate energy definitions introduced in the preceding section the calculation of energy at node $(i, j)$ involves the nodal values of nearest neighbors, as per Equations 11 and 15. As a consequence, positive energy release upon redistribution cannot be ensured simply by adjusting the threshold value in the LH93 instability criterion (3). However, it is possible to retain a stability criterion of the general form:

$$\Delta A_{i,j} > \alpha Z_c, \qquad (16)$$

by modifying the definition of the curvature $\Delta A_{i,j}$. As detailed in Appendix A, these new curvature definitions involve varying numbers of next-nearest neighbors to node $(i, j)$ in Equation 16. These new curvature formulae, together with their corresponding energy "quantum" $e_0$, are compiled in Table 1. The corresponding curvature stencils are displayed in Figure 7 in the Appendix A, together with the notational definition for nearest-neighbors sets $N_1, N_2$, etc.

**Table 1.** Curvature equation $\Delta A_{i,j}$ and smallest energy increment $e_0$ for three energy definitions.

|  | $\Delta A_{i,j}$ | $e_0$ | Equation |
|---|---|---|---|
| $A^2$ | $1.6A_{i,j} - 0.4\sum N_1$ | $0.8(2\alpha - 1)Z_c^2$ | 1, 20 |
| $B^2$ | $1.6A_{i,j} - 0.3\sum N_1 - 0.4\sum N_3 + 0.1\sum N_4$ | $0.76(2\alpha - 1)Z_c^2$ | 33 |
| $AJ$ | $4A_{i,j} - 1.6\sum N_1 + 0.4\sum N_2 + 0.2\sum N_3$ | $2.24(2\alpha - 1)Z_c^2$ | 42 |

With these new energy and curvature definitions, we can build internally consistent avalanche models. However, since we are using different curvature stencils, two adjustments have been made.

- First, as the new stencils probe wider than the closest lattice neighbors, the curvature computation requires additional boundary conditions at the lattice edge. For the $B^2$ model, we simply pad the lattice with zeros. For the $AJ$ model, we pad the lattice with negative nodal values so as to keep $J = 0$ on the boundary. These choices are explained in detail in Appendix A.1.
- Second, instead of requiring that $|\Delta A_{i,j}| > Z_c$, we require that $\Delta A_{i,j} > Z_c$ as the $AJ$ model is prone to cases where neighbor nodes with opposite curvatures simultaneously redistribute which reverses the curvatures and create and alternating checkerboard patterns. This can lead to the development of very long avalanches, effectively locking the model into a non-SOC state. We note that this adjustment is only necessary for the $AJ$ model, and that applying it to the $A^2$ and $B^2$ models does not affect their statistics. For the sake of consistency, we have opted to apply this rule to all the models in what follows.

## 4.2. Results

Since the models now have different boundary conditions and stability criteria, the self-organised criticality state they reach differs substantially. Examples of energy releases and lattice energy for the models are displayed in Appendix A.5. Figure 3A shows the absolute pile height in the form of 1D slices through lattice center, while panel B shows the pile height normalized to its peak central value, for models run under our three distinct energy definition and associated stability criteria (viz. Table 1). Both the absolute pile height and shape are very different. The absolute pile height is determined by the stability criterion, since in the statistically stationary non-avalanching state the average curvature is typically a set fraction of the stability threshold value. The pile shape is affected by both the adopted stability criterion and associated boundary condition. The absolute pile height is actually not important dynamically, since in the self-organised critical state the unfolding of avalanches is determined primarily by the distribution of curvature measures over the lattice, as plotted on Fig. 3C. Despite very different pile heights and shapes, the $A^2$ and $B^2$ models have closely similar curvature distributions, while that of the $AJ$ model differs more significantly. As we shall presently see, this translates into distinct distributions of event size measures.
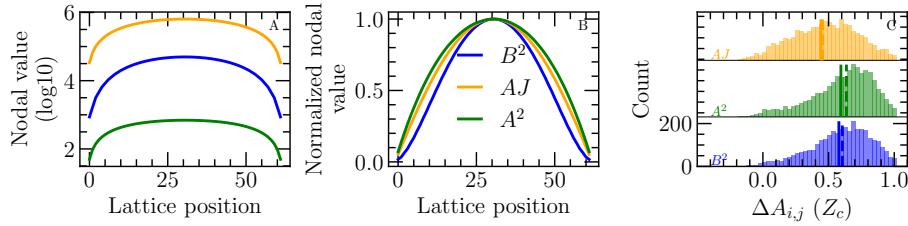


**Figure 3.** [A] and [B] Transversal slice across lattice center of the nodal value in models with different definitions of energies. [A] The log10 of the nodal value. [B] The nodal value divided by the maximum value along the slice. [C] Histogram of the curvature at lattice nodes for each model. For each histogram, the mean (solid line) and median (dashed line) are displayed.

Some statistical properties of avalanche have observational equivalents in solar flares: the total energy released by the avalanche ($E$), the maximal energy released in one iteration of an avalanche ($P$) and the duration of avalanches ($T$). For each model, we collect those parameters for each avalanche that occurred over $10^7$ iterations and build their frequency distributions, as shown on Figure 4. In all models, $E$ and $P$ are expressed in units of the quantum $e_0$, as listed in Table 1. To recover the power-law exponent for each distribution, we fit the complementary cumulative distribution function as detailed in Appendix C. The values for all power-law indices and associated error bars in this paper are provided in Table 2. The corresponding power law exponents are listed in each panel.

The remarkable similarity of the event size distributions for the $A^2$ and $B^2$ models is a direct reflection of their similar distributions of curvature measures (see Fig. 3C). This confirms that the choice of $A^2$ or $B^2$ as an energy definition in these models leads to equivalent distribution of energy release, provided that
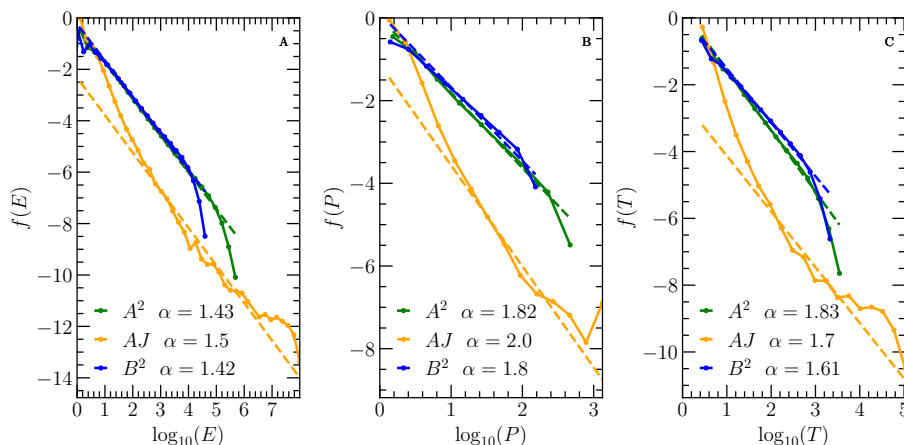
**Figure 4.** Probability distribution of avalanche sizes in the L93 avalanche model run under our three different energy definitions. [A] The energy dissipated by avalanches. [B] The peak energy dissipated by avalanches. [C] The duration of avalanches. For each model, a dashed line is used as a visual guide for the logarithmic slope $\alpha$ computed with the method detailed in Appendix C. All models are run on a 64x64 lattice with $\delta A \in [-0.2, 0.8]$.

the model rules are formulated in a manner consistent with the adopted energy definition. It is also clear from figure 4 that the $AJ$ model differs significantly from the other two in its statistical properties. It exhibits slightly steeper power law slopes in $(E)$ and $(P)$, but not as steep as the slopes reported by Farhang, Safari, and Wheatland (2018). This steeper power law is again consistent with the curvature distributions in figure 3: fewer lattice nodes are close to the stability threshold, which makes it harder for large avalanches to develop. The event size distributions from this model also extend to higher values of total energies, peak energy and durations.

## 5. Energy Minimization in Redistribution

In the solar flare context, a *sine qua non* requirement is that avalanches should release energy, by reducing the system's energy content. Farhang, Safari, and Wheatland (2018) have pushed this logic one step further by designing a lattice-based avalanche model in which redistribution locally *minimizes* lattice energy, thus maximizing energy release. Reaching the lowest available energy state is the hallmark of closed systems relaxing to equilibrium, which can arguably be applied locally to magnetic reconnection since the associated dynamical timescales are much shorter than those characterizing the global evolution of active regions.

We follow here Farhang, Safari, and Wheatland (2018) in introducing redistribution rules in which the amount of nodal variable transferred to nearest-neighbors upon redistribution are no longer the same, unlike the isotropic redistribution characterizing the original LH93 model (viz. Equation 4). For simplicity, we first retain the $A^2$-based definition of magnetic energy (Section 5.1), and consider two formulations of energy-minimizing redistribution: the original

analytical method introduced by Farhang, Safari, and Wheatland (2018) (hereafter F18), and a variation based on a Monte Carlo approach (MC). In both cases redistribution is restricted to the four immediate nearest-neighbors, as in the original LH93 model. Then, we extend the MC approach to the two other definitions of energy considered in this work ($AJ$ and $B^2$, Section 3)

### 5.1. Analytical Maximization of the Energy Release

The energy-minimizing, anisotropic redistribution rule introduced by Farhang, Safari, and Wheatland (2018) is defined as:

$$
\begin{aligned}
A'_{i,j} &= A_{i,j} - \frac{4Z_c}{5}, \\
A'_{i+1,j} &= A_{i+1,j} + \frac{r_1}{x+a}\frac{Z_c}{5}, \\
A'_{i-1,j} &= A_{i-1,j} + \frac{r_2}{x+a}\frac{Z_c}{5}, \\
A'_{i,j+1} &= A_{i,j+1} + \frac{r_3}{x+a}\frac{Z_c}{5}, \\
A'_{i,j-1} &= A_{i,j-1} + \frac{x}{x+a}\frac{Z_c}{5},
\end{aligned}
\tag{17}
$$

where $a = r_1 + r_2 + r_3$ and $r_1, r_2, r_3$ are random numbers extracted from a uniform distribution $\in [0,1]$, controlling the amount of nodal variable transferred to three of the nearest-neighbour nodes. The idea is then to choose a value for $x$, which sets the quantity of nodal variable transferred to the fourth nearest-neighbour node, in a manner such as to minimize lattice energy after the redistribution. In Equations 17 this fourth node was chosen as $(i, j-1)$, but in practice the optimization direction must be chosen randomly at each redistribution, in order to ensure global isotropy in avalanching behavior. The calculation of this optimal $x$ is detailed in Appendix B (see Equation 50), in the context of the $A^2$ definition of energy.

Following the methodology of Farhang, Safari, and Wheatland (2018), the optimal $x$ is obtained following a variational approach. Nevertheless, this approach leads to some situations that need to be treated with care. First, the variational approach only guarantees that $x$ is an extremum value, but not necessarily always a maximum. Second, if the optimal $x$ is negative, situations where $x \approx -a$ will destabilize the system as an arbitrarily large amount of nodal value can be distributed to the neighbors. When such situations occur, we generate new sets of $r_k$ in a new random direction each time until $x > 0$ and is an actual maximum. Typically, up to 20 trials are required to achieve this.

### 5.2. Monte Carlo Maximization of the Energy Release

A Monte Carlo approach to lattice energy minimization can also be designed based on the anisotropic redistribution rule introduced in Strugarek *et al.* (2014):

$$
A'_{i,j} = A_{i,j} - \frac{4Z_c}{5},
\tag{18}
$$

$$A'_{N_1} = A_{N_1} + \frac{r_k}{a}\frac{4Z_c}{5}, \qquad k = 1, 2, 3, 4. \tag{19}$$

with $a = \sum r_k$ and the four $r_k$'s $\in [0, 1]$ are again uniformly distributed random numbers. The idea is then to generate $N_{MC}$ sets of $r_k$'s, calculate for each the energy that would be released upon redistribution, and retain the set member that leads to the lowest post-redistribution lattice energy (i.e. the largest energy release). Note that even in the $N_{MC} \to \infty$ limit this approach does *not* become identical to the Farhang, Safari, and Wheatland (2018) scheme of Section 5.1, since in this latter case only the amount $x$ of nodal variable transferred in the selected optimization direction is varied to achieve minimization of lattice energy in a given redistribution event; whereas in the Monte Carlo scheme all four nearest-neighbour increments are reset randomly at each of the $N_{MC}$ minimization trial. As a consequence, the Farhang, Safari, and Wheatland (2018) model tends to generate redistributions that are more strongly anisotropic, and does not minimize lattice energy as much as the Monte Carlo scheme can, already at $N_{MC} = 20$.

### 5.3. Comparison of the Optimized Models

We now compare and contrast simulation runs carried out under both energy minimization schemes, to a "standard" LH93 run using the isotropic redistribution (4). All simulations are carried out on a $64 \times 64$ lattice, with $Z_c = 1$ and forcing amplitude $\delta A \in [-0.2, 0.8]$, under the original energy definition (6).
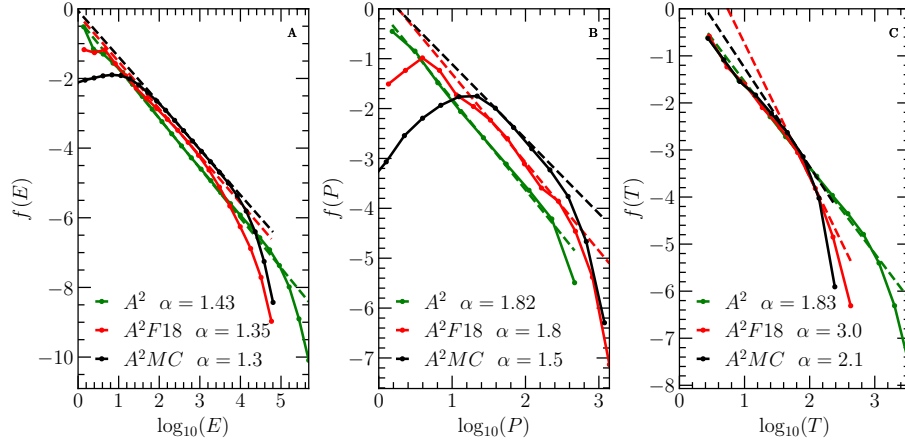


**Figure 5.** Probability distribution of avalanche sizes in the L93 avalanche model with 64x64 size and $A^2$ definition of energy. LH is the standard non optimized model. F18 is the analytical optimized model and MC is the Monte-Carlo optimized model. For each model, a dashed line is used as a visual guide for the logarithmic slope $\alpha$ computed with the method detailed in Appendix C. All models have $\delta A \in [-0.2, 0.8]$ and have a fixed stability threshold and restriction for the curvature $\Delta > Z_c$.

Interestingly, the power-law indices characterizing avalanche size measures are similar between all three models. However, as shown in Figure 5, the ranges

of frequency distributions for these size measures are altered by energy minimization. As was to be expected, the peak energy release (panel B) is larger in both energy minimizing models, and avalanche durations (panel C) are markedly reduced, a consequence of lattice energy dropping more rapidly during avalanches developing under either energy minimization schemes. These trends are slightly more pronounced with the Monte Carlo-based minimization, which is to be expected since it samples a broader range of potential post-redistribution lattice states. It is interesting to note that neither of the optimized models are able to produce avalanches with total energy as large as the LH model (panel A). This occurs because under either energy minimization schemes, even small avalanches are more efficient at reducing lattice energy, making it more difficult for energy to accumulate in the lattice and give rise, upon destabilization, to very large avalanches. Finally, note that the MC model is so efficient at releasing energy that even small avalanches of only one or two nodes usually release a relatively large amount of energy, i.e., many times the quantum $e_0$. This depletes the distribution of energy released at small values, leading to the break of scale invariance at low energy, characterizing the MC model on panels A and B.

### 5.4. Optimization Under the Different Energy Definitions

We now apply the MC minimization approach to models constructed under our three energy definitions. The statistical properties of those models are shown in Figure 6. Comparing to Figure 4, it is clear that within the MC framework, the differences between the event size distributions under the three different energy definition models are much reduced. This suggests that the steeper power-law indices, as first reported in Farhang, Safari, and Wheatland (2018), are associated with the $AJ$ energy definition, rather than with the energy release maximization procedure.

Figure 6 also suggests that redistribution rules maximizing energy release, when pushed to their limit, do succeed in releasing as much energy as can possibly be released by the lattice, under any plausible definition of lattice energy. This would be akin the free energy of coronal magnetic structures, corresponding to the magnetic energy above that of a potential magnetic field satisfying the same boundary conditions (see, e.g., Aly, 1991).

## 6. Discussion and Conclusion

The primary appeal of self-organised critical avalanche models remains their robust reproduction of the power-law form of the statistics of event size measures. However, going beyond the power-law form towards quantitative comparison of model predictions to observations requires an unambiguous definition of lattice and avalanche energies, as an essential step in bridging the gap between such simple statistical models, the magnetohydrodynamics of solar flares, and actual flare observations.

In this paper, working with a two-dimensional variation on the original Lu *et al.* (1993) avalanche model, we have investigated this question under three
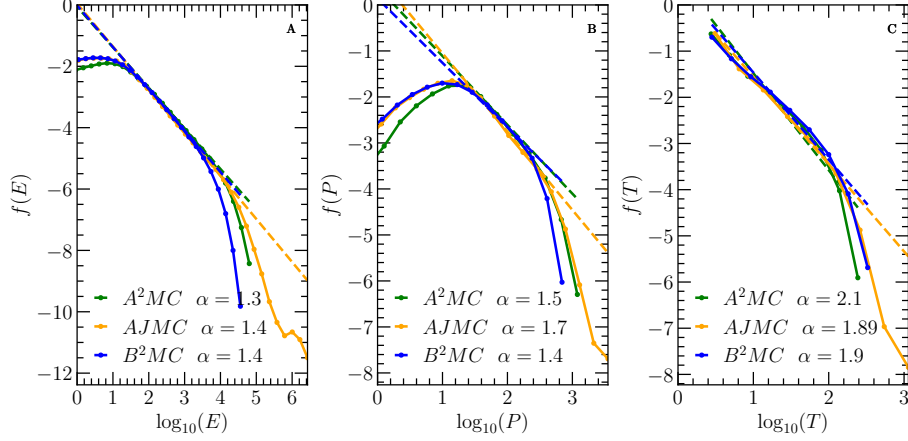
**Figure 6.** Statistical properties of three Monte Carlo optimized models with $64 \times 64$ size for the $A^2$, $B^2$ and $AJ$ definition of energy. For each model, a dashed line is used as a visual guide for the logarithmic slope $\alpha$ computed with the method detailed in Appendix C. All models have $\delta A \in [-0.2, 0.8]$ and have a fixed stability threshold and restriction for the curvature $\Delta > Z_c$.

physically plausible definitions of lattice energy, all expressed in term of a nodal variable identified with a magnetic vector potential. The first equates lattice energy to the sum of the squared vector potential; the second computes a magnetic field $\mathbf{B} = \nabla \times \mathbf{A}$ via finite difference evaluation of the curl operator on the lattice, and then equates energy to $B^2$ summed over all lattice nodes. The third is the alternate energy magnetic definition introduced by Farhang, Safari, and Wheatland (2018), which computes energy as $\mathbf{A} \cdot \mathbf{J}$ summed over the lattice, $\mathbf{J}$ being the electric current density, again computed through finite differences over the lattice. Under the geometrical setup and physical interpretation of our 2D lattice and exact mathematics, these second and third definitions are in principle identical.

A *sine qua non* requirement of SOC avalanche models is that once a node exceeds the instability threshold, redistribution must (1) locally restore stability at that node, and (2) release lattice energy (see, e.g., Lu, 1995b). We have shown that in order for both of these conditions to be systematically satisfied, the choice of a specific energy definition must be accompanied by a consistent definition of redistribution rules and/or stability criterion accompanied by specifying boundary conditions. Failing to do so results in avalanching nodes sometimes releasing "negative" energy and/or remaining unstable after redistribution, with significant consequences on the dynamical behavior and pattern of energy release. This ends up forcing the introduction of *ad hoc* and physically dubious additional procedures to yield a functional model.

Running the Lu *et al.* (1993) under the these three energy definitions and appropriately defined stability criteria yields avalanche statistics, i.e. distributions of total avalanche energy, duration and peak energy release, that are almost indistinguishable in the case of the $A^2$ and $B^2$ energy definitions. This vindicates, a posteriori, the common use of the summed squared nodal variable as a measure

of lattice energy (e.g. Lu *et al.*, 1993; Georgoulis and Vlahos, 1998; Strugarek and Charbonneau, 2014; Morales and Santos, 2020; Thibeault *et al.*, 2022).

We have also explored a physically appealing proposal, also put forth by Farhang, Safari, and Wheatland (2018), namely that redistribution should not just release lattice energy, but in fact *maximize* the amount of magnetic energy released during a redistribution. We have investigated two implementations of this idea, the first essentially identical to the procedure introduced by Farhang, Safari, and Wheatland (2018), the other based on a Monte Carlo optimisation scheme. The latter is more demanding computationally, but turns out to achieve higher levels of energy release than the original optimization scheme of Farhang, Safari, and Wheatland (2018). Indeed, the Monte Carlo scheme is so efficient that it exhibits a pronounced deficit of single-node avalanches of very small energies, causing a break of scale invariance at these energies. Excluding these smallest avalanches, under such energy maximization schemes, avalanches are typically more intense (higher peak energy release), of shorter duration, but release similar total amounts of energy.

An appealing property of the energy minimizing avalanche models first proposed by Farhang, Safari, and Wheatland (2018); Farhang, Wheatland, and Safari (2019) is their ability to generate steeper power laws in the size measures of energy release events, in better agreement with current observational inferences (see, e.g., Aschwanden and Parnell, 2002; Joulin *et al.*, 2016; Vilangot Nhalil *et al.*, 2020). Working under their *AJ* energy definition within the classical L93 model, i.e., without maximizing energy release, we recover slightly steeper power-law slopes (viz. Figure 4) albeit not as steep as the one reported by Farhang, Safari, and Wheatland (2018). This difference likely stems from our implementation of this energy definition, which differs significantly, especially with regard to the stability criterion (Section 4.1). However, applying the two schemes for energy maximization to the L93 model yields similar power-law slopes as non-energy-maximizing isotropic redistribution (see Figure 5). Moreover, the modelling results presented in Section 5.4 also indicate that even under the *AJ* energy definition the steeper power-law slopes of Figure 4 revert to those characterizing the other energy definitions upon imposing the strong minimization achieved by the Monte Carlo optimization scheme (cf. Figure 6). One can thus conclude that steeper power-law slopes in event size measures do not directly result from the maximization of energy release. Our modelling results suggest instead that the key is a broad curvature distribution, characterized by relatively few lattice nodes being very close to the instability threshold (viz. Figure 3C). The Farhang, Safari, and Wheatland (2018) model happens to achieve this through the combination of their energy definition and specific choices of update rules.

In general, closed systems near equilibrium are expected to minimize their energy in seeking equilibrium; however, a flaring active region is not a closed system, is likely far from equilibrium, and the reconfiguration of the magnetic field is subjected to topological constraints posed by MHD invariants such as magnetic helicity. Whether or not a flaring site within an active region can really relax to a locally minimal energy state (consistent with boundary conditions) is an extremely interesting physical question, which remains entirely open at this juncture.

# Appendix

## A. Curvature Definitions

We present here the detailed calculations leading to the curvature definitions and energy quantas presented in Table 1, Section 4. The goal is to ensure the decrease of lattice energy during redistribution. We opted to retain the nearest-neighbour redistribution rule (4) and a stability criterion of the general form (16), but alter the definition of curvature $\Delta A_{i,j}$ according to the energy definition adopted.

### A.1. Curvature Stencils and Boundary Conditions

The new curvature expressions for the two alternate energy definitions introduced in Section 3 end up involving more nodal neighbours than under the original energy definition (6) used in L93. Figure 7 depicts the stencils and associated notation used in this appendix to describe the new curvature formulae.
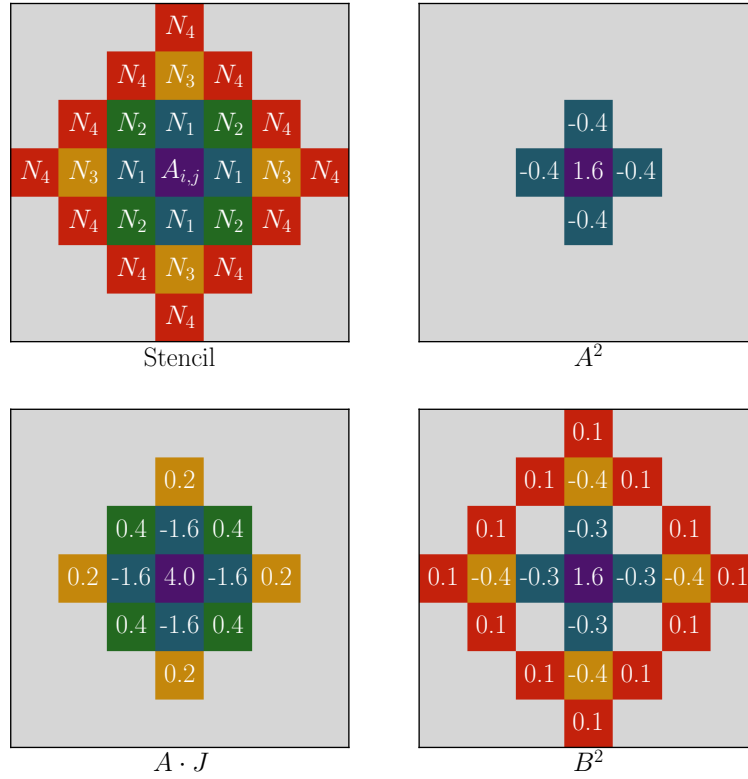


**Figure 7.** Visualisation of the different curvature stencils. Each of them applies to a curvature inequation of the form $\Delta A_{i,j} > Z_c$ where $\Delta A_{i,j}$ is a weighted sum over all cells, with weights given in the stencils. Empty cells are not used for calculation of the curvature $\Delta A_{i,j}$.

As with the original L93 model, under all energy definitions the nodal variable $A_{i,j}$ is reset to zero at every (avalanching) iteration on all boundary nodes.

In view of the driving and use of conservative redistribution rules, this is a *sine qua non* condition for reaching a statistically stationary state. This is the only boundary condition required in the $A^2$ model. However, the wider stencils used along with the $B^2$ and $AJ$ energy definitions require additional boundary conditions.

For the $B^2$ stencil, one $N_3$ and three $N_4$ neighbours lie outside the lattice when applying the curvature stencil to an interior node adjacent to the lattice boundary. Additional $N_3$ and $N_4$ are involved when considering the four interior corner nodes. We opted to simply pad the lattice with two layers of ghost nodes, on which $A = 0$ is enforced at all times.

In the case of the $AJ$ stencil, one $N_3$ neighbour can lie outside the lattice, with two additional $N_3$ nodes in the case of internal corner nodes. However, simply padding the lattice with a layer of $A = 0$ ghost nodes leads to $J$ changing sign when moving from the edge of the lattice to the center, while $A$ remains positive. Under the $AJ$ energy definition (14), this produces an annular region adjacent to the lattice boundaries where nodes contribute *negatively* to lattice energy. This is clearly an unphysical situation, which moreover ends up affecting significantly the statistics of event size measures in this model. Motivated by our physical/geometrical picture (viz. Section 2.2), we require instead that the current $J$ be zero on the lattice boundary, as required in the vacuum exterior to a coronal loop. This is achieved setting the value of $A$ at each ghost nodes equal to the negative of the value of its corresponding interior node, as per Equation 15. All interior nodes then contribute positively to lattice energy.

Under these boundary conditions, edge nodes have zero energy in the $A^2$ and $AJ$ models. This condition is not striclty achieved in the $B^2$ models, but their contribution to lattice energy remains insignificant.

## A.2. Stability Rule for $A^2$ Model.

Consider a single node $(i, j)$ exceeding the instability threshold and redistributing to its nearest neighbors according to the rule (4). Under the energy definition (6), the change in lattice energy denoted $\Delta E_A$ is

$$
\begin{aligned}
\Delta E_A &= \left( A_{i,j}^2 + \sum A_{N_1}^2 \right) - \left( (A_{i,j} - \frac{4}{5} Z_c)^2 + \sum (A_{N_1} + \frac{1}{5} Z_c)^2 \right) \\
&= \frac{4}{5} Z_c \left( 2 A_{i,j} - \frac{1}{2} \left( A_{i+1,j} + A_{i-1,j} + A_{i,j+1} + A_{i,j-1} \right) - Z_c \right) \\
&= \frac{4}{5} Z_c \left( 2 \Delta A_{i,j} - Z_c \right),
\end{aligned}
\tag{20}
$$

the last step making use of the curvature definition (1) and $N_1$ corresponding to the four neighbors depicted in Figure 7B. A positive energy release $\Delta E_A > 0$ thus leads to the constraint (9):

$$
\Delta A_{i,j} > \frac{1}{2} Z_c.
\tag{21}
$$

This constraint can be generalized in the form

$$\Delta A_{i,j} > \alpha Z_c, \tag{22}$$

with $\alpha > 1/2$. The minimal energy release "quantum" $e_0$ is then obtained when $\Delta A_{i,j} = \alpha Z_c$ and is given by

$$e_0 = \frac{4}{5}(2\alpha - 1)Z_c^2. \tag{23}$$

This generic formulation reduces to Equation 8 for $\alpha = 1$.

The redistribution must also restore stability. Consider a situation where node $(i,j)$ is barely below the instability threshold, i.e.:

$$A_{i,j} - \frac{1}{4}\sum_{N_1} A_{N_1} = \alpha Z_c - \epsilon, \tag{24}$$

with $\epsilon \ll \alpha Z_c$. Upon adding an increment $\delta A$ ($> \epsilon$) to $A_{i,j}$, the instability threshold is exceeded and redistribution takes place. Post-redistribution, the curvature should be reduced below $\alpha Z_c$:

$$\left(A_{i,j} + \delta A - \frac{4}{5}Z_c\right) - \frac{1}{4}\left(\sum_{N_1} A_{N_1} + \frac{1}{5}Z_c\right) < \alpha Z_c,$$

$$A_{i,j} + \delta A - \frac{4}{5}Z_c - \frac{1}{4}\sum_{N_1} A_{N_1} - \frac{1}{5}Z_c < \alpha Z_c,$$

$$A_{i,j} - \frac{1}{4}\sum_{N_1} A_{N_1} + \delta A - Z_c < \alpha Z_c,$$

$$\alpha Z_c - \epsilon + \delta A - Z_c < \alpha Z_c, \tag{25}$$

where (24) was used in the last step. Even with $\epsilon \ll 1$, stability is always restored provided the increments $\delta A$ is small enough to satisfy:

$$\delta A < Z_c. \tag{26}$$

### A.3. Stability Rule for $B^2$ Model.

Similarly, for the $\mathbf{B}^2$ energy definition, consider a single node $(i,j)$ exceeding the instability threshold and redistributing to its nearest neighbors according to the rule (4). Under the energy definition (10), (11), the change in lattice energy denoted $\Delta E_B$ is

$$\Delta E_B = \left(B_{i,j}^2 + \sum B_{N_1}^2 + \sum B_{N_2}^2 + B_{N_3}^2\right) - \left(B_{i,j}'^2 + \sum B_{N_1}'^2 + \sum B_{N_2}'^2 + B_{N_3}'^2\right), \tag{27}$$

where $N_1$, $N_3$ and $N_4$ are the three groups of neighbors, as displayed in Figure 7D. We can expand this expression by detailing the energy evolution over single

nodes. First we have

$$
\begin{aligned}
B_{i,j}^2 - B_{i,j}'^2 &= (A_{i-1,j} - A_{i+1,j})^2 + (A_{i,j-1} - A_{i,j+1})^2 - \\
&\quad (A_{i-1,j} + \frac{1}{5}Z_c - A_{i+1,j} - \frac{1}{5}Z_c)^2 - \\
&\quad (A_{i,j-1} + \frac{1}{5}Z_c - A_{i,j+1} - \frac{1}{5}Z_c)^2 \\
&= 0
\end{aligned}
\tag{28}
$$

Then, for the energy of a $B_{N_1}$ node, we show an example of derivation for $B_{i,j+1}$ (the computation is similar for the other nodes):

$$
\begin{aligned}
B_{i,j+1}^2 - B_{i,j+1}'^2 &= (A_{i-1,j+1} - A_{i+1,j+1})^2 + (A_{i,j} - A_{i,j+2})^2 - \\
&\quad (A_{i-1,j+1} - A_{i+1,j+1})^2 - (A_{i,j} - \frac{4}{5}Z_c - A_{i,j+2})^2 \\
&= Z_c \left( 1.6 A_{i,j+2} - 1.6 A_{i,j} - 0.64 Z_c \right).
\end{aligned}
\tag{29}
$$

Similarly, for the energy of a $B_{N_2}$ node we obtain

$$
\begin{aligned}
B_{i+1,j+1}^2 - B_{i+1,j+1}'^2 &= (A_{i,j+1} - A_{i+2,j+1})^2 + (A_{i+1,j} - A_{i+1,j+2})^2 \\
&\quad -(A_{i,j+1} - \frac{1}{5}Z_c - A_{i+2,j+1})^2 - \\
&\quad (A_{i+1,j} - \frac{1}{5}Z_c - A_{i+1,j+2})^2 \\
&= Z_c \left( 0.4(A_{i+1,j+2} + A_{i+1,j} + A_{i+2,j+1} + A_{i,j+1}) \right. \\
&\quad \left. - 0.08 Z_c \right).
\end{aligned}
\tag{30}
$$

Finally, for the energy of a $B_{N_3}$ node:

$$
\begin{aligned}
B_{i,j+2}^2 - B_{i,j+2}'^2 &= (A_{i-1,j+2} - A_{i+1,j+2})^2 + (A_{i,j} - A_{i,j+3})^2 \\
&\quad -(A_{i-1,j+2} - A_{i+1,j+2})^2 - (A_{i,j+1} - \frac{4}{5}Z_c - A_{i,j+3})^2 \\
&= Z_c \left( 0.4 A_{i,j+3} - 0.4 A_{i,j+1} - 0.4 Z_c \right).
\end{aligned}
\tag{31}
$$

Computing the energy difference in this manner for each stencil node and assembling the results, we obtain:

$$
\begin{aligned}
\Delta E_B &= 0.76 Z_c \left( \frac{1}{0.76} \left[ 1.6 A_{i,j} - 0.3 \sum A_{N_1} - 0.4 \sum A_{N_3} + 0.1 \sum A_{N_4} \right] - Z_c \right) \\
&= 0.76 Z_c \left( 2 \Delta_B A_{i,j} - Z_c \right),
\end{aligned}
\tag{32}
$$

where we have introduced $\Delta_B A_{i,j}$ defined as

$$
\Delta_B A_{i,j} = \frac{1}{1.52} \left[ 1.6 A_{i,j} - 0.3 \sum A_{N_1} - 0.4 \sum A_{N_3} + 0.1 \sum A_{N_4} \right].
\tag{33}
$$

Similarly to case $A^2$ (Appendix A.2), a positive energy release $\Delta E_B > 0$ can be expressed as

$$\Delta_B A_{i,j} > \frac{1}{2} Z_c. \tag{34}$$

We can, again, generalize this criterion to $\Delta_B A_{i,j} > \alpha Z_c$, with $\alpha > 1/2$. When $\alpha = 1$, we recover the energy release quantum

$$e_0 = 0.76 Z_c \left(2 Z_c - Z_c\right) = 0.76 Z_c^2. \tag{35}$$

The redistribution must also restore stability. Consider a situation where a node $(i,j)$ is barely below the instability threshold, i.e.:

$$\frac{1}{1.52} \left[ 1.6 A_{i,j} - 0.3 \sum A_{N_1} - 0.4 \sum A_{N_3} + 0.1 \sum A_{N_4} \right] = \alpha Z_c - \epsilon \tag{36}$$

Consider now a node receiving an driving increment $\delta A$, and subsequently redistributing. We require that the new curvature is below the instability threshold:

$$\frac{1}{1.52} \left[ 1.6 \left( A_{i,j} + \delta A - \frac{4}{5} Z_c \right) - 0.3 \sum \left( A_{N_1} + \frac{1}{5} Z_c \right) - \right.$$
$$\left. 0.4 \sum A_{N_3} + 0.1 \sum A_{N_4} \right] < \alpha Z_c \tag{37}$$

$$\alpha Z_c - \epsilon + \frac{1}{1.52} \left( 1.6 \delta A - 0.3 \frac{4}{5} Z_c - 1.6 \frac{4}{5} Z_c \right) < \alpha Z_c \tag{38}$$

$$-\epsilon + \delta A < 0.95 Z_c, \tag{39}$$

where (36) was used in the last step. Even with $\epsilon \ll 1$, stability is always restored provided the increments $\delta A$ is small enough to satisfy:

$$\delta A < 0.95 Z_c. \tag{40}$$

### A.4. Stability Rule for *AJ* Model.

Moving on to the *AJ* energy definition, consider again a single node $(i,j)$ exceeding the instability threshold and redistributing to its nearest neighbors according to the rule (4). Under the energy definition (14), (15), the change in lattice energy, denoted $\Delta E_{AJ}$, is

$$\Delta E_{AJ} = \left( A_{i,j} J_{i,j} + \sum A_{N_1} J_{N_1} + \sum A_{N_2} J_{N_2} + \sum A_{N_3} J_{N_3} \right)$$
$$- \left( A'_{i,j} J'_{i,j} + \sum A'_{N_1} J'_{N_1} + \sum A'_{N_2} J'_{N_2} + \sum A'_{N_3} J'_{N_3} \right) \ , .$$

where $N_1$, $N_2$ and $N_3$ are the neighbors as displayed in figure 7C. Following the same methodology as in A.3, we break down the various parts of the expression

of $\Delta E_{AJ}$ to obtain

$$
\begin{aligned}
A_{i,j}J_{i,j} - A'_{i,j}J'_{i,j} &= \frac{1}{2}A_{i,j}\left(4A_{i,j} - \sum A_{N_1}\right) \\
&\quad - \frac{1}{2}\left(A_{i,j} - \frac{4}{5}Z_c\right)\left(4\left(A_{i,j} - \frac{4}{5}Z_c\right) - \sum\left(A_{N_1} + \frac{1}{5}Z_c\right)\right) \\
&= Z_c\left(3.6A_{i,j} - 0.4\sum A_{N_1} - 1.6Z_c\right).
\end{aligned}
$$

As an example, we detail the energy change for node $A_{i,j+1}J_{i,j+1}$ belonging to the $N_2$ group (the calculation is similar for the other nodes) and obtain

$$
\begin{aligned}
A_{i,j+1}J_{i,j+1} - A'_{i,j+1}J'_{i,j+1} &= \frac{1}{2}A_{i,j+1}\left(4A_{i,j+1} - A_{i,j+2} - A_{i,j} - A_{i+1,j+1} - A_{i-1,j+1}\right) \\
&\quad - \frac{1}{2}\left(A_{i,j+1} + \frac{1}{5}Z_c\right)\left[4\left(A_{i,j+1} + \frac{1}{5}Z_c\right)\right. \\
&\quad \left. - A_{i,j+2} - A_{i,j} + \frac{4}{5}Z_c - A_{i+1,j+1} - A_{i-1,j+1}\right] \\
&= Z_c\left[0.2(A_{i,j} + A_{i,j+2} + A_{i-1,j+1} + A_{i+1,j+1})\right. \\
&\quad \left. - 2.4A_{i,j+1} - 0.32Zc\right].
\end{aligned}
$$

Computing the energy difference for each node and assembling the results yields:

$$
\begin{aligned}
\Delta E_{AJ} &= 2.24Z_c\left(\frac{1}{2.24}\left[4A_{i,j} - 1.6\sum_{N_1} A_{N_1} + 0.2\sum_{N_2} A_{N_2} + 0.4\sum_{N_3} A_{N_3}\right] - Zc\right) \\
&= 2.24Z_c\left(2\Delta_J A_{i,j} - Z_c\right),
\end{aligned} \tag{41}
$$

where we have defined

$$
\Delta_J A_{i,j} = \frac{1}{4.48}\left[4A_{i,j} - 1.6\sum_{N_1} A_{N_1} + 0.2\sum_{N_2} A_{N_2} + 0.4\sum_{N_3} A_{N_3}\right]. \tag{42}
$$

A positive energy release $\Delta E_{AJ} > 0$ therefore requires

$$
\Delta_J A_{i,j} > \frac{1}{2}Z_c. \tag{43}
$$

Again, we can generalize this criterion to $\Delta_J A_{i,j} > \alpha Z_c$, and for $\alpha = 1$, we recover the quantum release of energy

$$
e_0 = 2.24Z_c\left(2Z_c - Z_c\right) = 2.24Z_c^2. \tag{44}
$$

The redistribution must also restore stability. Consider a node $(i,j)$ barely below the instability threshold,

$$
\frac{1}{4.48}\left[4A_{i,j} - 1.6\sum_{N_1} A_{N_1} + 0.2\sum_{N_2} A_{N_2} + 0.4\sum_{N_3} A_{N_3}\right] = \alpha Z_c - \epsilon, \tag{45}
$$

receiving a driving increment $\delta A$, and then redistributing. We require that the new curvature be below the instability threshold:

$$\alpha Z_c > \frac{1}{4.48}\left[\ 4\left(A_{i,j} + \delta A - \tfrac{4}{5}Z_c\right) - 1.6\sum_{N_1}\left(A_{N_1} + \tfrac{1}{5}Z_c\right) + \right.$$
$$\left. 0.2\sum_{N_2}A_{N_2} + 0.4\sum_{N_3}A_{N_3}\right], \tag{46}$$

$$\alpha Z_c - \epsilon + \frac{1}{4.48}\left(4\delta A - 1.6\frac{4}{5}Z_c - 4\frac{4}{5}Z_c\right) < \alpha Z_c, \tag{47}$$

$$-\epsilon + \delta A < 1.12 Z_c. \tag{48}$$

where (45) was used in the last step. Even with $\epsilon \ll 1$, stability is always restored provided the increments $\delta A$ is small enough to satisfy:

$$\delta A < 1.12 Z_c. \tag{49}$$

### A.5. Characteristic Patterns of Energy Release

With the new curvature definitions and boundary conditions, under the action of random forcing each model eventually reaches a SOC state. However, these equilibrium states are characterized by distinct dynamics. For example, the $AJ$ model exhibits a unique class of rare, large avalanches. Figure 8 displays the characteristic patterns of energy release for each model described in Section 4. The left panels show the evolution of the energy of the lattices and the energy release over an extended time span, whereas the right panels zoom in on the shaded region in the left panels, spanning now only 1000 iterations. The $A^2$ and $B^2$ models are qualitatively similar, but the $AJ$ model stands distinct from the other two. Nonetheless, all three models exhibit typical SOC behavior in their pattern of intermittent energy release and power-law form of their event size measures.

## B. Analytical Optimization of Energy Release in $A^2$ models

We detail in what follows the analytical calculation underlying the redistribution maximizing energy release in the LH model under its conventional $A^2$ energy definition (Section 5.3 and Figure 5). We start from the redistribution rules introduced by Farhang, Safari, and Wheatland (2018), as given by Equations 17 in Section 5.1.

The optimal $x$ maximizing energy release is calculated via a variational approach, namely by solving $\mathrm{d}\Delta E/\mathrm{d}x = 0$ for $x$:

$$\frac{d}{dx}\Delta E = -\frac{d}{dx}(A_{i,j}'^2 + A_{i+1,j}'^2 + A_{i-1,j}'^2 + A_{i,j+1}'^2 + A_{i,j-1}'^2)$$
$$0 = 2\left[\left(A_{i+1,j} + \frac{4Z_c r_1}{5(x+a)}\right)\left(\frac{4Z_c r_1}{5(x+a)^2}\right) + \left(A_{i-1,j} + \frac{4Z_c r_2}{5(x+a)}\right)\left(\frac{4Z_c r_2}{5(x+a)^2}\right)\right.$$
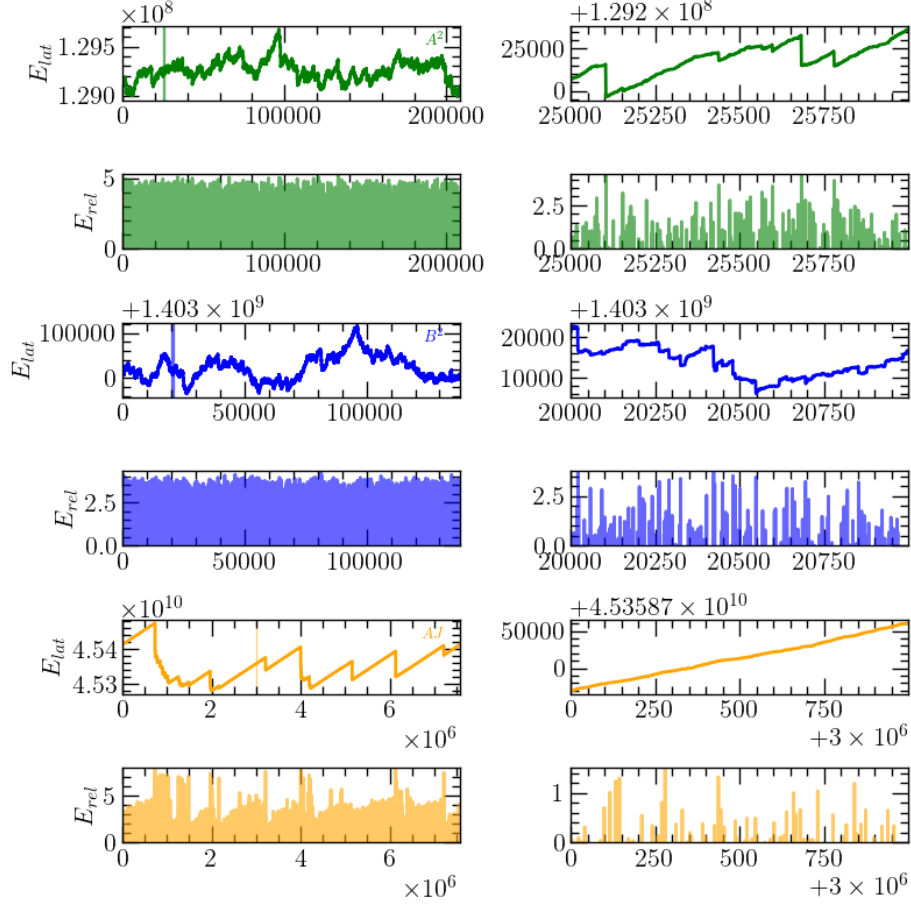
**Figure 8.** Lattice energy and released energy for the $A^2$, $B^2$ and $AJ$ models. The number of iterations displayed are different for each model and chosen for clarity of the plots.

$$+ \left( A_{i,j+1} + \frac{4Z_c r_3}{5(x+a)} \right) \left( \frac{4Z_c r_3}{5(x+a)^2} \right) - \left( A_{i,j-1} + \frac{4Z_c x}{5(x+a)} \right) \left( \frac{4Z_c a}{5(x+a)^2} \right) \right]$$

$$0 = \frac{8Z_c}{5(x+a)^2} \left[ r_1 \left( A_{i+1,j} + \frac{4Z_c r_1}{5(x+a)} \right) + r_2 \left( A_{i-1,j} + \frac{4Z_c r_2}{5(x+a)} \right) \right.$$

$$\left. + r_3 \left( A_{i,j+1} + \frac{4Z_c r_3}{5(x+a)} \right) - a \left( A_{i,j-1} + \frac{4Z_c x}{5(x+a)} \right) \right].$$

The above equation reduces to

$$0 = \underbrace{r_1 A_{i+1,j} + r_2 A_{i-1,j} + r_3 A_{i,j+1} - a A_{i,j-1}}_{\Theta} + \underbrace{\frac{4Z_c}{5}}_{C} \overbrace{\frac{r_1^2 + r_2^2 + r_3^2 - ax}{x+a}}^{\Phi}$$

$$0 = \Theta + \frac{C}{(x+a)}\left(\Phi - ax\right) \ ,$$

where we have introduced the new variables $\Theta$, $C$, and $\Phi$ that are independent of $x$ to ease the notations. We can now solve for $x$ to obtain

$$x = \frac{C\Phi + \Theta a}{-\Theta + Ca} \ . \tag{50}$$
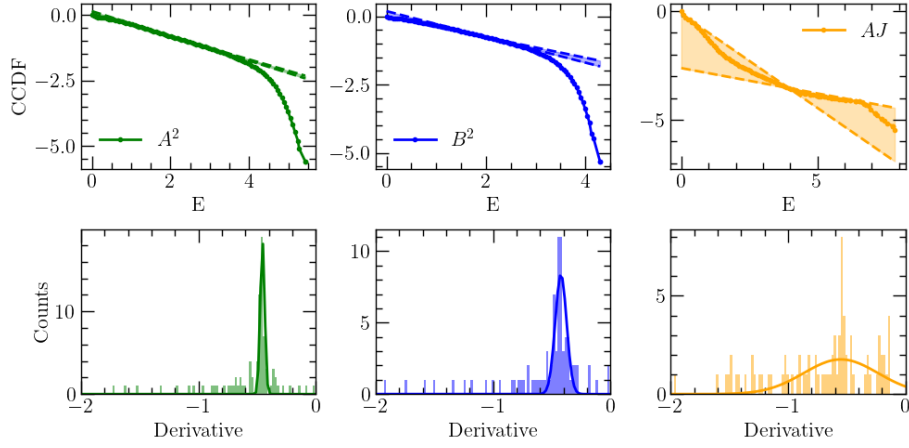
## C. Power-law Indices



**Figure 9.** [Top] Complementary cumulative distribution functions (CCDF) for the energy release of each model defined in section 4. A $1\sigma$ span of $\alpha_{ccdf}$ is shown as an visual guide for each CCDF as a shaded region within dashed lines. [Bottom] Histograms of the slopes of the CCDF and their gaussian best fits are displayed for each model.

**Table 2.** Reported values for the power law slope $\alpha$ of each model presented in this paper.

| Model | $\alpha_E$ | $\alpha_P$ | $\alpha_T$ |
|---|---|---|---|
| $A^2$ | $1.43 \pm 0.02$ | $1.82 \pm 0.08$ | $1.83 \pm 0.02$ |
| $B^2$ | $1.42 \pm 0.05$ | $1.8 \pm 0.2$ | $1.61 \pm 0.03$ |
| $AJ$ | $1.5 \pm 0.5$ | $2.0 \pm 1.0$ | $1.7 \pm 0.6$ |
| $A^2 F18$ | $1.35 \pm 0.06$ | $1.8 \pm 0.4$ | $3.0 \pm 1.0$ |
| $A^2 MC$ | $1.3 \pm 0.3$ | $1.5 \pm 0.6$ | $2.1 \pm 0.2$ |
| $B^2 MC$ | $1.4 \pm 0.3$ | $1.4 \pm 0.05$ | $1.9 \pm 0.2$ |
| $AJMC$ | $1.4 \pm 0.2$ | $1.7 \pm 0.7$ | $1.9 \pm 0.2$ |

Deriving power-law exponents is generally done by specifying arbitrary boundaries for the fitting interval. However, for smoothly varying distributions, the selection of these bounds introduce biases. To alleviate this pitfall, we develop here a method for computing power-law indices without setting arbitrary bounds.

We begin by computing the complementary cumulative distribution function (CCDF). This function is generally smoother than the PDF since the latter requires binning of the data. The power-law slope for the CCDF is related to the power-law slope of the PDF by:

$$\alpha = 1 - \alpha_{ccdf} \, , \qquad (51)$$

where $\text{PDF}(X) = X^\alpha$ for any quantity $X$. In order to find $\alpha_{ccdf}$, we sample the slope of the CCDF along a logarithmic scale to avoid giving too much weight to zones with higher point density. We then create a histogram of the slope values and fit that distribution with a Gaussian function, as shown in Figure 9 for $E$ of models $A^2$, $B^2$ and $AJ$. In order to reduce the uncertainty caused by the tail of the distribution, the Gaussian function is recursively fitted by ignoring bins outside $3\sigma$ of the mean until the mean converges within $0.01\%$. The value and uncertainty for $\alpha_{ccdf}$ are then reported as the mean and width of the Gaussian. This method attributes large uncertainties for distributions with significant deviations from a singular power-law, such as the $AJ$ model in Figure 4, panel C. The values for $\alpha$ for each model, with associated error bars, are listed in Table 2.

# References

Aly, J.J.: 1991, How Much Energy Can Be Stored in a Three-dimensional Force-free Magnetic Field? *The Astrophysical Journal Letters* **375**, L61. DOI. ADS.

Aschwanden, M.J.: 2011, *Self-Organized Criticality in Astrophysics*. ADS.

Aschwanden, M.J.: 2013, *Self-Organized Criticality Systems*. ADS.

Aschwanden, M.J., Parnell, C.E.: 2002, Nanoflare statistics from first principles: fractal geometry and temperature synthesis. *The Astrophysical Journal* **572**(2), 1048.

Bak, P., Tang, C., Wiesenfeld, K.: 1988, Self-organized criticality. *Physical Review A* **38**(1), 364. DOI. ADS.

Bélanger, E., Vincent, A., Charbonneau, P.: 2007, Predicting Solar Flares by Data Assimilation in Avalanche Models. I. Model Design and Validation. *Solar Physics* **245**(1), 141. DOI. ADS.

Charbonneau, P., McIntosh, S.W., Liu, H.-L., Bogdan, T.J.: 2001, Avalanche models for solar flares (invited review). *Solar Physics* **203**(2), 321.

Dennis, B.R.: 1985, Solar Hard X-Ray Bursts. *Solar Physics* **100**, 465. DOI. ADS.

Farhang, N., Safari, H., Wheatland, M.S.: 2018, Principle of Minimum Energy in Magnetic Reconnection in a Self-organized Critical Model for Solar Flares. *The Astrophysical Journal* **859**(1), 41. DOI. ADS.

Farhang, N., Wheatland, M.S., Safari, H.: 2019, Energy Balance in Avalanche Models for Solar Flares. *The Astrophysical Journal Letters* **883**(1), L20. DOI. ADS.

Georgoulis, M.K., Vlahos, L.: 1998, Variability of the occurrence frequency of solar flares and the statistical flare. *Astronomy and Astrophysics* **336**, 721. ADS.

Hughes, D., Paczuski, M., Dendy, R.O., Helander, P., McClements, K.G.: 2003, Solar Flares as Cascades of Reconnecting Magnetic Loops. *The Physical Review Letters* **90**(13), 131101. DOI. ADS.

Isliker, H., Anastasiadis, A., Vlahos, L.: 2000, MHD consistent cellular automata (CA) models. I. Basic features. *Astronomy and Astrophysics* **363**, 1134. ADS.

Isliker, H., Anastasiadis, A., Vassiliadis, D., Vlahos, L.: 1998, Solar flare cellular automata interpreted as discretized MHD equations. *Astronomy and Astrophysics* **335**, 1085. ADS.

Jensen, H.J.: 1998, *Self-organized criticality: emergent complex behavior in physical and biological systems* **10**, Cambridge university press, Cambridge.

Joulin, V., Buchlin, E., Solomon, J., Guennou, C.: 2016, Energetic characterisation and statistics of solar coronal brightenings. *Astronomy and Astrophysics* **591**, A148.

Liu, H.-L., Charbonneau, P., Pouquet, A., Bogdan, T., McIntosh, S.: 2002, Continuum analysis of an avalanche model for solar flares. *Physical Review E* **66**(5), 056111. DOI. ADS.

López Fuentes, M.C., Klimchuk, J.A.: 2010, A Simple Model for the Evolution of Multi-stranded Coronal Loops. *The Astrophysical Journal* **719**(1), 591. DOI. ADS.

Lu, E.T.: 1995a, Avalanches in Continuum Driven Dissipative Systems. *The Physical Review Letters* **74**(13), 2511. DOI. ADS.

Lu, E.T.: 1995b, The Statistical Physics of Solar Active Regions and the Fundamental Nature of Solar Flares. *The Astrophysical Journal Letters* **446**, L109. DOI. ADS.

Lu, E.T., Hamilton, R.J.: 1991, Avalanches and the Distribution of Solar Flares. *The Astrophysical Journal Letters* **380**, L89. DOI. ADS.

Lu, E.T., Hamilton, R.J., McTiernan, J.M., Bromund, K.R.: 1993, Solar Flares and Avalanches in Driven Dissipative Systems. *The Astrophysical Journal* **412**, 841. DOI. ADS.

Masuda, S., Kosugi, T., Hara, H., Tsuneta, S., Ogawara, Y.: 1994, A loop-top hard X-ray source in a compact solar flare as evidence for magnetic reconnection. *Nature* **371**(6497), 495. DOI. ADS.

Morales, L., Charbonneau, P.: 2008, Self-organized Critical Model of Energy Release in an Idealized Coronal Loop. *The Astrophysical Journal* **682**(1), 654. DOI. ADS.

Morales, L.F., Santos, N.A.: 2020, Predicting Extreme Solar Flare Events Using Lu and Hamilton Avalanche Model. *Solar Physics* **295**(11), 155. DOI. ADS.

Parker, E.N.: 1988, Nanoflares and the Solar X-Ray Corona. *The Astrophysical Journal* **330**, 474. DOI. ADS.

Robinson, P.A.: 1994, Scaling properties of self-organized criticality. *Physical Review E* **49**(5), 3919. DOI. ADS.

Shibata, K., Magara, T.: 2011, Solar flares: magnetohydrodynamic processes. *Living Reviews in Solar Physics* **8**(1), 1.

Strugarek, A., Charbonneau, P.: 2014, Predictive Capabilities of Avalanche Models for Solar Flares. *Solar Physics* **289**(11), 4137. DOI. ADS.

Strugarek, A., Charbonneau, P., Joseph, R., Pirot, D.: 2014, Deterministically driven avalanche models of solar flares. *Solar Physics* **289**. ISBN 978-1-4939-2037-2. DOI.

Thibeault, C., Strugarek, A., Charbonneau, P., Tremblay, B.: 2022, Forecasting Solar Flares by Data Assimilation in Sandpile Models. *arXiv e-prints*, arXiv:2206.13583. ADS.

Tsuneta, S., Hara, H., Shimizu, T., Acton, L.W., Strong, K.T., Hudson, H.S., Ogawara, Y.: 1992, Observation of a Solar Flare at the Limb with the YOHKOH Soft X-Ray Telescope. *Publications of the Astronomical Society of Japan* **44**, L63. ADS.

Vilangot Nhalil, N., Nelson, C.J., Mathioudakis, M., Doyle, J.G., Ramsay, G.: 2020, Power-law energy distributions of small-scale impulsive events on the active sun: results from iris. *Monthly Notices of the Royal Astronomical Society* **499**(1), 1385.